Post-conversion sialylation of prions in lymphoid tissues

Saurabh Srivastava[a,b], Natallia Makarava[a,b], Elizaveta Katorcha[a,b], Regina Savtchenko[a,b], Reinhard Brossmer[c], and Ilia V. Baskakov[a,b,1]

[a]Center for Biomedical Engineering and Technology, University of Maryland School of Medicine, Baltimore, MD 21201; [b]Department of Anatomy and Neurobiology, University of Maryland School of Medicine, Baltimore, MD 21201; and [c]Biochemistry Center, University of Heidelberg, 69120 Heidelberg, Germany

Edited by Ajit Varki, University of California at San Diego, La Jolla, CA, and accepted by the Editorial Board October 21, 2015 (received for review September 11, 2015)

Sialylated glycans on the surface of mammalian cells act as part of a "self-associated molecular pattern," helping the immune system to recognize "self" from "altered self" or "nonself." To escape the host immune system, some bacterial pathogens have evolved biosynthetic pathways for host-like sialic acids, whereas others recruited host sialic acids for decorating their surfaces. Prions lack nucleic acids and are not conventional pathogens. Nevertheless, prions might use a similar strategy for invading and colonizing the lymphoreticular system. Here we show that the sialylation status of the infectious, disease-associated state of the prion protein (PrP^{Sc}) changes with colonization of secondary lymphoid organs (SLOs). As a result, spleen-derived PrP^{Sc} is more sialylated than brain-derived PrP^{Sc}. Enhanced sialylation of PrP^{Sc} is recapitulated in vitro by incubating brain-derived PrP^{Sc} with primary splenocytes or cultured macrophage RAW 264.7 cells. General inhibitors of sialyltranserases (STs), the enzymes that transfer sialic acid residues onto terminal positions of glycans, suppressed extrasialylation of PrP^{Sc}. A fluorescently labeled precursor of sialic acid revealed ST activity associated with RAW macrophages. This study illustrates that, upon colonization of SLOs, the sialylation status of prions changes by host STs. We propose that this mechanism is responsible for camouflaging prions in SLOs and has broad implications.

prions | prion diseases | sialic acid | sialylated glycans | macrophages

Prions are proteinaceous infectious agents that lack nucleic acids (1, 2). Mammalian prions replicate by recruiting the normal cellular form of the prion protein (PrP), denoted as PrP^{C}, and converting it into the disease-associated form, denoted as PrP^{Sc} (3). Although the central nervous system (CNS) represents the main site of PrP^{Sc} replication and deposition, PrP^{Sc} is also found in peripheral organs, including cells and organs of the lymphoreticular system (4–7). Not only does PrP^{Sc} colonize secondary lymphoid organs (SLOs), the germinal centers of spleen and lymph nodes offer suitable environments for replicating PrP^{Sc} autonomously from the CNS (8–11). Prion colonization and replication in SLOs is important for several reasons. First, for prions acquired via peripheral routes, colonization of SLOs precedes invasion of the CNS (12–14). Second, SLOs are more permissive to prions acquired via cross-species transmission than the CNS (15). As such, the lymphoreticuar system represents a silent reservoir of infection, where prions could hide undetected while imposing a high risk of transmission through blood donation (16, 17). Finally, chronic inflammation could expand distribution of prions to inflamed tissues that are usually not affected by prions under normal conditions (18, 19).

PrP^{C} is a sialoglycoprotein in which terminal sialic acids are attached to galactose residues of two *N*-linked glycans via α2–3 and α2–6 linkages (20–22). The ratio of diglycosylated to monoglycosylated and unglycosylated PrP^{C} glycoforms increases with neuronal differentiation (23), yet the role of *N*-linked glycans and their sialylation for PrP^{C} function is unknown. Upon conversion to PrP^{Sc}, the posttranslational modifications of PrP^{C}, including its *N*-linked glycans, are carried over, giving rise to sialylated PrP^{Sc} (24, 25). The sialylation status of brain-derived PrP^{Sc} was found to closely resemble that of PrP^{C} (25). In mammals, sialic acids are the most abundant terminal residues of cell membrane glycans. Sialic acids play an essential role in a broad range of cellular functions, but are especially important for neuronal plasticity and immunity (26). Among other functions, sialic acids on the surface of mammalian cells act as a part of a "self-associated molecular pattern," helping the immune system to recognize "self" from "altered self" or "nonself" (27). A decline in sialic acid content represents one of the molecular signatures of "apoptotic-cell-associated molecular patterns" found in apoptotic or aging cells (28, 29). Removal of sialic acids from cell surface glycans exposes galactose residues that generate "eat me" signals for professional and nonprofessional macrophages. Examples include clearance of erythrocytes or platelets with reduced sialic acid residues by Kupffer cells (30, 31) or apoptotic neurons by microglia (32, 33). Pathogens without sialic acids are more likely to be detected as foreign, by virtue of recognition of their nonsialylated glycans that contribute to "pathogen-associated molecular patterns" and also because of the lack of the protective effects of sialic acids (34). In a striking illustration of molecular mimicry, a number of bacterial pathogens, including *Escherichia coli* K1 and group B *Streptococcus*, evolved enzymes to synthesize and express host-like sialic acids on their surfaces (34). Although ∼20% of the prokaryotic genomes sequenced evolved genes responsible for biosynthesis of sialic acids or their analogs (35), a number of pathogens, including *Trypanosoma cruzi*, *Corynebacterium diphtheriae,*

Significance

In mammals, sialic acids are the most abundant terminal residues on cell-surface glycans and comprise "self-associated molecular patterns," which protect the host from inappropriate activation of multiple immune pathways. In a striking illustration of molecular mimicry, a number of microbial pathogens recruit host sialic acids to decorate their surfaces and hide from the same immune responses. Prions are proteinaceous infectious agents, not conventional pathogens. This study found that sialylation of prions is enhanced upon their colonization of secondary lymphoid organs, via extracellular host sialylation machinery. Thus, prions may use strategies similar to other pathogens to camouflage themselves from the immune system, facilitating host invasion.

Author contributions: S.S., N.M., E.K., and I.V.B. designed research; S.S., N.M., E.K., and R.S. performed research; R.B. contributed new reagents/analytic tools; S.S., N.M., E.K., and I.V.B. analyzed data; and I.V.B. wrote the paper.

The authors declare no conflict of interest.

This article is a PNAS Direct Submission. A.V. is a guest editor invited by the Editorial Board.

Freely available online through the PNAS open access option.

[1]To whom correspondence should be addressed. Email: baskakov@umaryland.edu.

This article contains supporting information online at www.pnas.org/lookup/suppl/doi:10.1073/pnas.1517993112/-/DCSupplemental.

Hemophilus influenzae, *Niesseria meningitides*, and others, recruit host sialic acid or its precursor to decorate their surfaces, presumably to hide from the immune system (34).

In the present study, we show that sialylation status of PrP^{Sc} is tissue-specific. Spleen-derived PrP^{Sc} was found to be more sialylated than brain-derived PrP^{Sc}. Enhanced sialylation of spleen-derived PrP^{Sc} occurred after conversion. Upon i.p. administration, the sialylation status of PrP^{Sc} sequestered in spleen changed within 6–24 h after injection. Enhanced sialylation of PrP^{Sc} could be recapitulated in vitro by incubating brain-derived PrP^{Sc} with primary splenocytes or cultured macrophage RAW cells. General inhibitors of sialyltranserases (STs), the enzymes that transfer sialic acid residues onto terminal positions, suppressed enhanced sialylation of PrP^{Sc}, suggesting that changes in PrP^{Sc} sialylation involve genuine ST activity. Application of a fluorescently labeled precursor of sialic acid revealed ST activity associated with RAW macrophages. Our data illustrate that, upon colonization of SLOs, prions alter their sialylation status by using host STs. We propose that this mechanism camouflages prions in SLOs and could account for the high permissiveness of SLOs to prions.

Results

Spleen-Derived PrP^{Sc} Is More Sialylated than Brain-Derived PrP^{Sc}. PrP^{Sc} particles are multimers that range greatly in size (36). To compare sialylation states of spleen- and brain-derived PrP^{Sc}, scrapie materials were treated with proteinase K (PK) to remove PrP^{C}, then denatured and analyzed by 2D gel electrophoresis (2D) (Fig. S1). In 2D, individual PrP molecules are separated according to their net charge in horizontal dimension. In PrP, each of the two *N*-linked glycans can carry up to five terminal sialic acid residues (21, 25), while an additional single sialic acid could be present on the glycosylphosphatidylinositol (GPI) anchor (37). Because individual PrP molecules contain from 0 to 10 sialic acids on their glycans, scrapie material is expected to display substantial charge heterogeneity (38). Indeed, PK-treated and denatured scrapie material showed multiple charge isoforms for both diglycosylated and monoglycosylated glycoforms (Fig. S1 and Fig. 1 *A*–*E*). Several charge isoforms were also seen for unglycosylated forms, a heterogeneity that is primarily attributed to the structural heterogeneity of the GPI-anchor (Fig. S1 and Fig. 1 *A*–*E*) (37). Nevertheless, as expected, the distribution of diglycosylated and monoglycosylated charged isoforms were shifted toward acidic pH relative to unglycosylated isoforms, and the heterogeneity of diglycosylated and monoglycosylated isoforms was much higher than that of unglycosylated forms. Both features are in agreement with glycan sialylation.

Animals were infected intracranially with mouse-adapted strains RML, ME7, and 22L; hamster-adapted strain 263K; or synthetic strain S05 (39), and their brain- and spleen-derived materials were analyzed by using 2D. Comparison of brain-derived materials revealed only minor strain- or species-specific differences in charged isoform distribution patterns (Fig. 1 *A*–*E*). Remarkably, regardless of the strain- or species-specific differences, brain-derived PrP^{Sc} glycoforms displayed a broader charge distribution than spleen-derived PrP^{Sc}, whereas spleen-derived diglycosylated glycoforms were shifted toward acidic pH relative to those of brain-derived glycoforms (Fig. 1 *A*–*E*). In contrast to diglycosylated glycoforms, unglycosylated glycoforms from spleen-derived material did not show acidic shift relative to the unglycosylated glycoforms from brain-derived material. With unglycosylated forms serving as internal references, acidic shift of diglycosylated isoforms indicates that the sialylation level of spleen-derived PrP^{Sc} was higher than that of brain-derived PrP^{Sc}. In animals inoculated intraperitoneally (i.p.), the sialylation patterns of spleen- or brain-derived PrP^{Sc} were very similar to those observed for animals inoculated intracranially, arguing that the spleen-specific sialylation pattern did not depend on the inoculation route (Fig. 1*A*). The spleen- and brain-specific

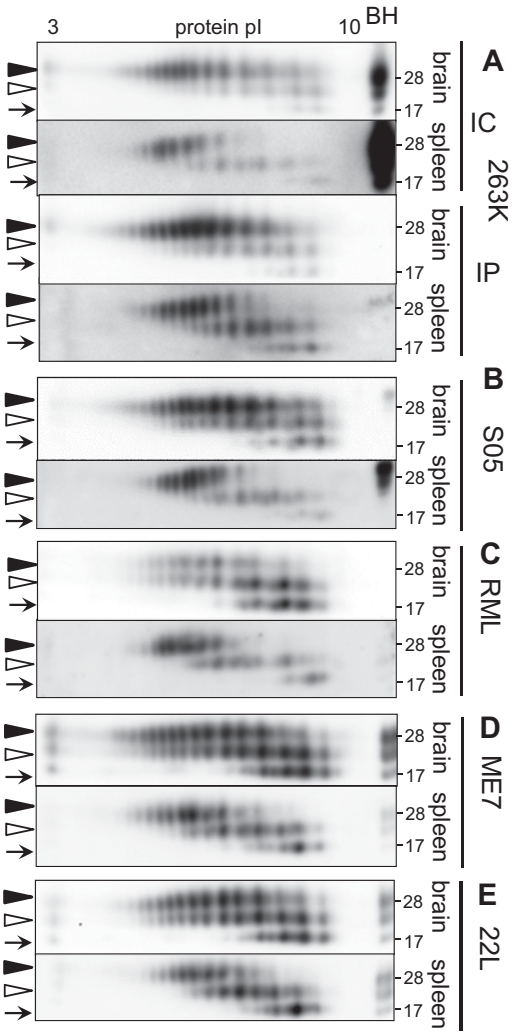

Fig. 1. The 2D analysis of brain- and spleen-derived materials. Shown is 2D analysis of PK-treated brain- and spleen-derived materials from animals infected with hamster-adapted strain 263K via i.c. or i.p. routes (*A*) or synthetic hamster strain S05 (*B*), mouse-adapted strains RML (*C*), ME7 (*D*), or 22L (*E*), all inoculated via i.c. Western blots were stained with 3F4 antibody for hamster or ab3531 for mouse. Filled and open triangles mark diglycosylated and monoglycosylated forms, respectively, and arrows mark unglycosylated forms. A marker lane shows PK-treated scrapie brain homogenate (BH).

2D patterns were highly reproducible within animal groups inoculated with the same strains (Fig. S2).

Differences in lengths of PK-resistant cores of PrP^{Sc} deposited in brain and spleen could contribute to differences in tissue-specific patterns of charged isoforms. PK cleaves PrP^{Sc} at multiple sites located within residues 74–102 (40, 41). Although distribution of sites is largely dependent on strain-specific structure, other parameters such as cleavage conditions and PK concentration could also affect site distribution (41, 42). Because the pI values of unglycosylated forms were the same for brain- and spleen-derived materials (Fig. 1 *A*–*E*), it is unlikely that differences in pI distribution of diglycosylated and monoglycosylated forms were due to different PK cleavage sites. Nevertheless, to determine the extent to which distribution of charge isoforms could be affected by digestion conditions, 263K brain-derived material was treated with 2, 20, or 200 μg/mL PK. An increase in PK concentration did not change the distribution of charge isoform on 2D (Fig. S3*A*). This experiment argues that, even if differences in PK-cleavage sites between

brain- and spleen derived materials exist, it is highly unlikely that such differences account for tissue-specific differences in 2D patterns.

To make sure that differences in charge distribution of brain- and spleen-derived materials were not due to the procedure used for preparation of spleen-derived PrP^{Sc}, normal spleen homogenate was spiked with brain-derived PrP^{Sc}, treated according to the procedure for spleen-derived PrP^{Sc}. Incubation of brain-derived PrP^{Sc} with spleen homogenate did not alter the brain-specific sialylation pattern of PrP^{Sc} (Fig. S3*B*). Finally, to confirm that charge distribution on 2D reports on sialylation status, brain- and spleen-derived materials were treated with acetic acid (Fig. S3*C*) or *Arthrobacter ureafaciens* sialidase (Fig. S3*D*), according to the protocols that remove sialic acid residues chemically or enzymatically, respectively. As expected, the charge distributions shifted toward basic pH in both brain- and spleen-derived materials in both control experiments (Fig. S3 *C* and *D*). In summary, the above experiments established that brain- and spleen-derived prions are different with respect to their sialylation status.

PrP^{Sc} Sequestered by Spleen Undergoes Sialylation. The higher level of sialylation of spleen- vs. brain-derived PrP^{Sc} could be due to (*i*) higher levels of sialylation of spleen- vs. brain-expressed PrP^{C}, (*ii*) additional sialylation of PrP^{Sc} deposited in spleens, and/or (*iii*) fast metabolic clearance of PrP^{Sc} particles with low sialylation levels in SLOs (Fig. 2 *A*–*C*). The last hypothesis assumes that subpopulations of differentially sialylated PrP^{Sc} particles—i.e., particles sialylated above or below statistically averaged level—exist. The first hypothesis was not supported by previous data illustrating that spleen-expressed PrP^{C} was equally or even less sialylated than brain-expressed PrP^{C} (38). To test the second and third hypotheses, we asked whether the sialylation status of PrP^{Sc} changes upon colonization of SLOs. Wild-type mice were inoculated i.p. by using brain-derived 263K, and sialylation status of PrP^{Sc} sequestered by cells of the peritoneal cavity, spleen, and mediastinal lymph nodes was tested 6 or 24 h after injection. Hamster-adapted strain 263K was used for inoculating mice to avoid interference due to immediate replication of mouse prions in mouse SLOs (43).

Relative to the charge isoform distribution of injected material, PrP^{Sc} recovered from all three sites (spleen, lymph nodes, and peritoneal cavity) showed isoform distribution shifted toward acidic pH on 2D by 24 h (Fig. 3). To analyze individual sialylation profiles, diglycosylated charge isoforms were separated arbitrarily into two categories, as described in *Materials and Methods*. Isoforms located toward acidic pH from pI 7.5 were designated as hypersialylated, and those toward basic pH were designated as hyposialylated (Fig. S1). The percentage of sum intensities of hypersialylated diglycosylated isoforms was used to estimate whether the shifts were statistically significant. PrP^{Sc} from spleen showed a more substantial shift than PrP^{Sc} sequestered by peritoneal cells or lymph nodes. Nevertheless, for all three sites, the shift toward acidic pH was statistically significant by 24 h after injection (Fig. 3). This result is in agreement with the hypothesis that PrP^{Sc} sequestered in SLOs is a substrate of STs and undergoes enhanced sialylation (Fig. 2*B*). However, this result cannot exclude the third hypothesis, according to which the acidic shift is due to faster clearance of PrP^{Sc} particles with low sialylation levels than particles with high sialylation levels (Fig. 2*C*).

If subpopulations of differentially sialylated PrP^{Sc} particles exist, they are expected to display a broad range of net charges. To test this, cation- and anion-exchange resins were used to isolate differentially charged and, therefore, differentially sialylated, PrP^{Sc} particles. Scrapie material was incubated with ion-exchange resins and then eluted by using increasing concentrations of NaCl (Fig. S4*A*). Peaks were eluted at 1.2 or 1.6 M NaCl from anion- or cation-exchange resins, respectively, and analyzed by using 2D. High concentrations of salt were required for eluting PrP^{Sc}, indicating that sorbtion of PrP^{Sc} to the resins was strong and depended on electrostatic interactions. Nevertheless, no differences with respect to the sialylation pattern were observed between

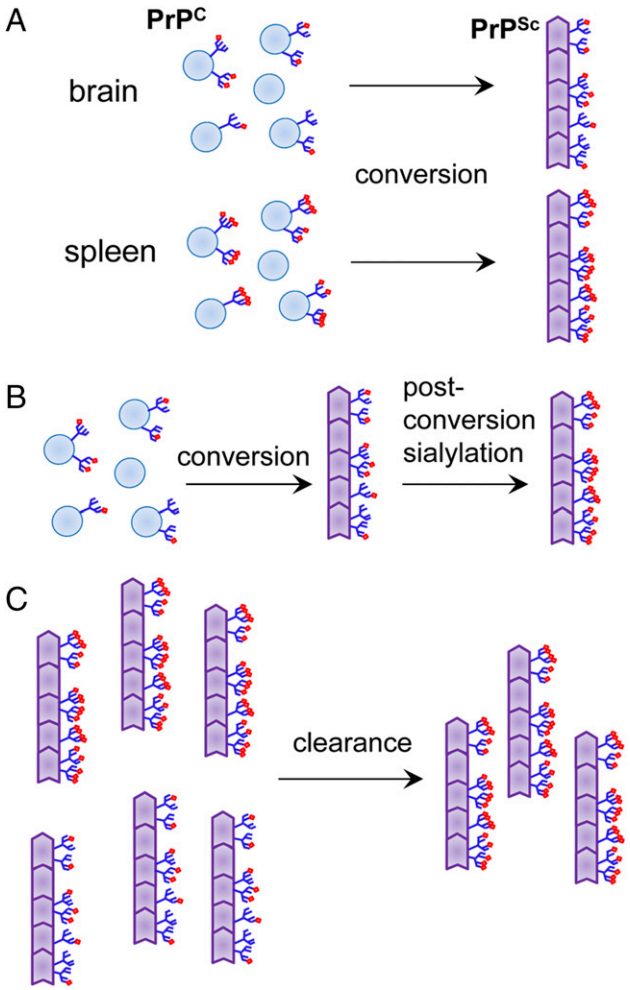

Fig. 2. Schematic diagram illustrating three alternative hypotheses. The higher level of sialylation of spleen- vs. brain-derived PrP^{Sc} could be due to the following reasons: Spleen-expressed PrP^{C} is sialylated at higher levels than brain-expressed PrP^{C} (*A*); PrP^{Sc} deposited in SLOs is sialylated by sialyltransferases (*B*); or, upon colonization of SLOs, PrP^{Sc} particles sialylated below the statistically average level are cleared faster than the PrP^{Sc} particles sialylated above the statistically average level (*C*). The third hypothesis assumes that differentially sialylated PrP^{Sc} particles exists. *N*-linked glycans are shown as blue lines, and terminal sialic acid residues are shown as red diamonds.

materials eluted from cation- or anion-exchange resins on 2D (Fig. S4*A*). In previous studies, PrP^{Sc} produced in Protein Misfolding Cyclic Amplification using desialylated PrP^{C} was found to be more sensitive to PK treatment than brain-derived PrP^{Sc} (38). We speculated that, if differentially sialylated PrP^{Sc} particles exist, they might have different physical properties, such as solubility or PK resistance. If this hypothesis is the case, fast proteolytic clearance of soluble, proteolytically sensitive PrP^{Sc} subfractions in SLOs could account for the acidic shifts on 2D. To test this hypothesis, 263K brain material was subjected to ultracentrifugation, and then the pellet and supernatant were analyzed by 2D. The distribution of charge isoforms was remarkably similar for PrP^{Sc} particles in both the pellet and supernatant (Fig. S4*B*). By using an alternative format, RML brain material was centrifuged according to the protocol that separates PK-sensitive and -resistant PrP^{Sc} particles (Fig. S4*C*). Again, no notable differences were observed in the distribution of charge isoforms between PK-sensitive and -resistant PrP^{Sc} (Fig. S4*C*). In summary, these results did not support the hypothesis that differentially sialylated PrP^{Sc}

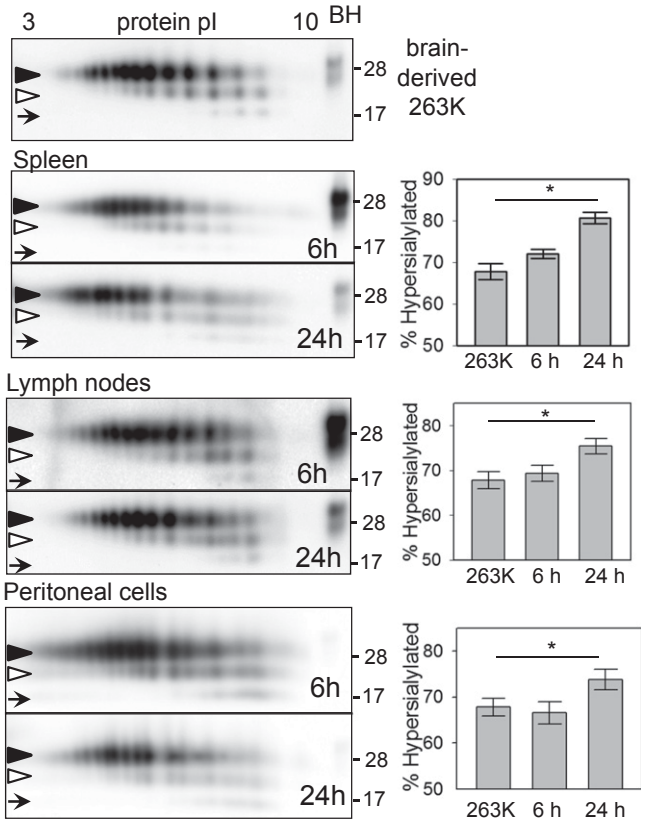

Fig. 3. PrP^{Sc} sequestered by SLOs undergoes sialylation. (*Left*) The 263K brain-derived material was administered i.p. to mice, and then scrapie material sequestered by cells of peritoneal cavity, lymph nodes, or spleen 6 or 24 h after injection was analyzed by 2D. (*Top*) The 2D analysis of the brain-derived 263K material used for IP injection is provided as a reference. (*Right*) Statistical analysis of sialylation status was performed as described in *Materials and Methods*. Data are presented as means ± SD. $*P < 0.05$ ($n = 3$). Western blots were stained with 3F4 antibody. Filled and open triangles mark diglycosylated and monoglycosylated forms, respectively, and arrows mark unglycosylated forms. Normal brain homogenate (BH) was loaded into the marker lane as a size reference.

particles exist within brain material. Instead, these data suggest that individual PrP^{Sc} particles consist of PrP molecules with a broad range of sialylation levels.

Primary Splenocytes, Peritoneal Cells, and Cultured Macrophages Sialylate PrP^{Sc}. To test whether PrP^{Sc} sialylation observed in vivo can be recapitulated in vitro, mouse splenocytes and peritoneal cells were isolated and cultured in vitro. Because macrophages are known to sequester and transport PrP^{Sc} to SLOs, the mouse macrophage RAW cell line was used in parallel experiments. Brain-derived PrP^{Sc} material was incubated with primary splenocytes, peritoneal cells, or RAW cells for 2 h, then cells were washed, medium was replaced (this time point is designated as 0 h), and the cells were cultured in fresh medium for 24 or 48 h. The distribution of PrP^{Sc} charge isoforms on 2D exhibited a notable, statistically significant shift toward acidic pH after 24 and 48 h in all cultured cells in comparison with the 0-h time points (Fig. 4 *A*–*D*). To make sure that this acidic shift was not due to a spontaneous "aging" or enzymatic activity that might be present in FBS, PrP^{Sc} was incubated in PBS alone or in the presence of FBS for 48 h in the absence of cells and assayed by 2D. No change in sialylation pattern was observed on 2D after 48 h of incubation in PBS or FBS (Fig. S5*A*). To rule out the possibility that PrP^{Sc} sialylation is due to sialyltransferases released by dead or spontaneously lysed cells, brain-derived PrP^{Sc} was incubated with cell medium collected after culturing confluent RAW cells for 48 h. Again, no change in sialylation pattern was observed on 2D (Fig. S5*B*). In another control experiment, brain-derived PrP^{Sc} materials were incubated with N2a cells, which are of neuronal origin, and probed by 2D. After 48 h of incubation, a very minor shift in the charge distribution was noticed, which was not statistically significant (Fig. S5*C*). These experiments established that the shift of PrP^{Sc} glycoforms toward acidic pH was due to cell-associated enzymatic activity and specific to splenocytes, peritoneal cells, or macrophages.

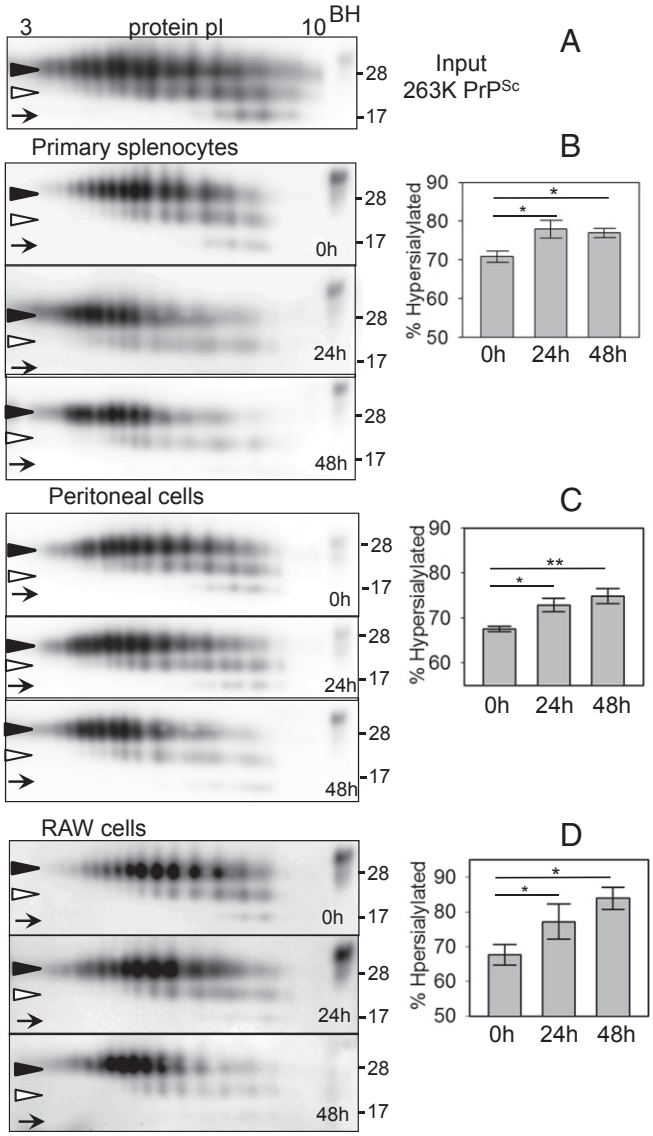

Fig. 4. Primary splenocytes and cultured macrophages sialylate PrP^{Sc}. The 263K brain-derived material (*A*) was incubated with primary splenocytes (*B*), peritoneal cells (*C*), or RAW cultured cells (*D*) for 2 h, and then scrapie material was removed, cells were rinsed, and culture medium was replaced. (*Left*) The sialylation status of 263K material sequestered by cells was analyzed at 0, 24, or 48 h of culturing cells after replacing the medium. (*Right*) Statistical analysis of sialylation status was performed as described in *Materials and Methods*. Data are presented as means ± SD. $*P < 0.05$; $**P < 0.005$ ($n = 3$). All Western blots were stained with 3F4 antibody. Filled and open triangles mark diglycosylated and monoglycosylated forms, respectively, and arrows mark unglycosylated forms. Normal brain homogenate (BH) was loaded into the marker lane as a size reference.

To confirm that the acidic shift in distribution of PrP^{Sc} glycoforms was due to ST activity, two general ST inhibitors, CTP and peracetylated $3F_{ax}$-Neu5Ac (FPN), were used (44–49). In the absence of inhibitors, the distribution of PrP^{Sc} charge glycoforms showed statistically significant shift toward acidic pH after incubation with RAW cells or primary splenocytes for 24 h as before (Fig. 5 *A* and *B*). However, in the presence of CTP or FPN, the changes in glycoform distribution patterns were very minor, if any, and not statistically different in comparison with the distribution at the 0-h time point (Fig. 5 *A* and *B*). This experiment confirmed that the shift in PrP^{Sc} glycoform distribution depends on genuine sialyltransferase activity.

RAW Macrophages Exhibit Sialyltransferase Activity. STs were traditionally thought to localize exclusively in Golgi (50). However, in a growing number of studies, ST activities were found on the surface of a wide variety of immune system cells (48, 49, 51–53). To test whether RAW cells exhibit surface ST activity, we used a fluorescently labeled precursor of sialic acid, CMP-5-FITC-neuraminic acid (CMP-5-FITC-NEU), which is a membrane-excluded and sialidase-resistant substrate (54). In the presence of CMP-5-FITC-NEU, RAW cells exhibited considerable fluorescence (Fig. 6). However, upon application of CTP, the fluorescence levels dropped more than fourfold (Fig. 6). When RAW cells were pretreated with bacterial neuraminidase, an enzyme

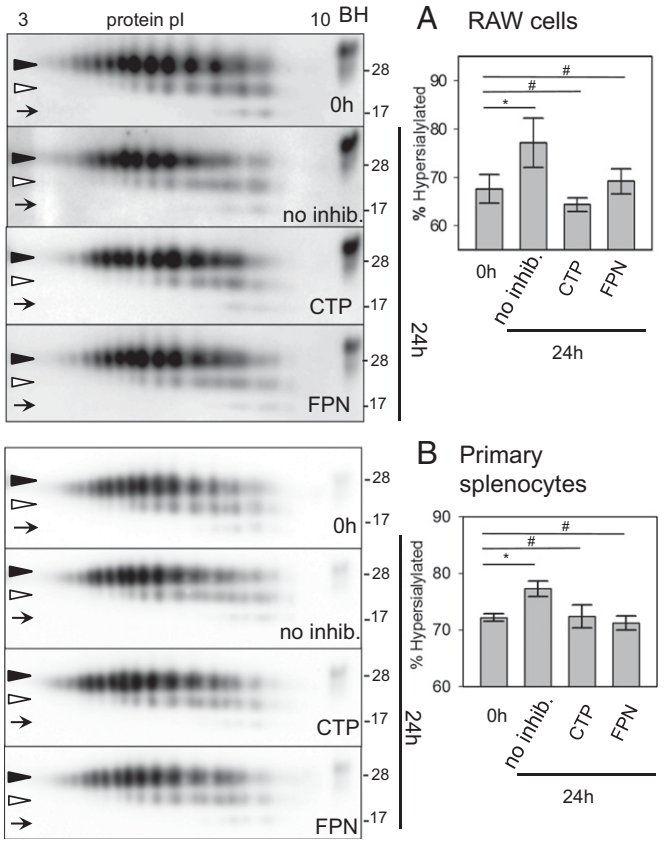

Fig. 5. ST inhibitors suppressed PrP^{Sc} sialylation. The 263K brain-derived material was incubated with RAW cells (*A*) or primary splenocytes (*B*) for 2 h, and then scrapie material was removed, and cells were rinsed and cultured for additional 24 h in the absence or presence of CTP or FPN inhibitors. (*Left*) The sialylation status was analyzed by 2D. (*Right*) Statistical analysis of sialylation status is performed as described in *Materials and Methods*. Data are presented as means ± SD. $*P < 0.05$; $\#P > 0.05$ ($n = 3$). All Western blots were stained with 3F4 antibody. Filled and open triangles mark diglycosylated and monoglycosylated forms, respectively, and arrows mark unglycosylated forms.

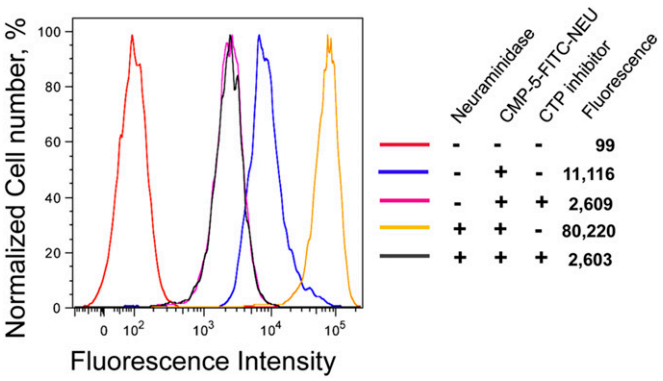

Fig. 6. Flow cytometry analysis of ST activity associated with RAW cells. Autofluorescence of RAW cells in the absence of CMP-5-FITC-NEU (red), RAW cells incubated with CMP-5-FITC-NEU (blue), or ST inhibitor CTP and CMP-5-FITC-NEU (magenta); cells pretreated with neuraminidase and then incubated with CMP-5-FITC-NEU (orange); or cells pretreated with neuraminidase and then incubated with CTP and CMP-5-FITC-NEU (black). The experiments were repeated twice.

that cleaves α2–3- and α2–6-linked sialic acid residues from cell surface glycoproteins and glycolypids, the cell-associated CMP-5-FITC-NEU fluorescence was sevenfold higher relative to the cells not treated with neuraminidase (Fig. 6). Remarkably, in the presence of CTP, the fluorescence level in neuraminidase-pretreated cells dropped by 30-fold from 80,220 to ~2,603 (Fig. 6). Although some of the fluorescence in the presence of CMP-5-FITC-NEU could be attributed to uptake and use of CMP-5-FITC-NEU by intracellular sialyltransferases, the strong effect of the ST inhibitor and pretreatment with bacterial neuraminidase argues that RAW cells display genuine ST activity on the cell surface. This result is consistent with previous studies that attributed CMP-5-FITC-NEU fluorescence to ST activity on the cell surface (48, 49).

Discussion

The present study provides, to our knowledge, the first experimental illustration that the primary structure of PrP^{Sc}—in particular, its sialylation status—is changed after conversion. Direct structural analysis of the *N*-linked glycoforms from spleen-derived and in vitro-produced materials with enhanced sialylation will be needed in future studies to define the details of what exactly is occurring. Nevertheless, enhanced sialylation of PrP^{Sc} was observed in SLOs regardless of prion strain, host species, or inoculation route tested. The alternative explanations to the hypothesis on postconversion sialylation are (*i*) that spleen-expressed PrP^{C} is sialylated at a higher level than the brain-derived PrP^{Sc} or (*ii*) fast metabolic clearance of PrP^{Sc} particles with low sialylation levels in SLOs (Fig. 2 *A* and *C*). The first alternative was not supported by the previous studies (38). The second alternative assumes that differentially sialylated PrP^{Sc} particles exist in brain-derived material. However, the experiments on fractionation of brain-derived PrP^{Sc} using three different methods did not support this hypothesis. Moreover, the model on differentially sialylated PrP^{Sc} particles assumes that PrP^{C} molecules are sorted out during PrP^{Sc} replication according to their sialylation status, where hyposialylated PrP^{C} would be recruited by hyposialylated PrP^{Sc} particles and hypersialylated PrP^{C} would be recruited by hypersialylated PrP^{Sc}, which is highly unlikely. Finally, experiments with sialyltransferease inhibitors linked the acidic shift of charged isoform distribution to sialyltransferase activity. Because sialylation plays multiple roles in immunity (26, 34), the present finding that spleen-deposited PrP^{Sc} is sialylated at higher levels than brain-derived PrP^{Sc} has broad implications.

Prions are not conventional pathogens, yet sialylation of prions in SLOs displays remarkable parallels with molecular mimicry of microbial pathogens. A number of pathogens decorate their surfaces by using host sialic acid in an attempt to hide from the immune system (34). Surfaces of mammalian cells and glycoproteins in blood circulation are densely sialylated (26). Sialylation represents a part of the self-associated molecular pattern used by cells of the immune system for recognizing self from altered self or nonself (28, 34). Similar to molecular mimicry of microbial pathogens, sialylation of prions in SLOs might play a similar role. This mechanism could be particularly important for cross-species prion transmission between mammals and human. Because of an irreversible mutation in the gene encoding *N*-acetylneuraminic acid hydroxylase that occurred during evolution from primates to human, the type of sialic acid produced in peripheral tissues of humans (*N*-acetyl neuraminic acid; Neu5Ac) is different from the type synthesized by other mammalian species (*N*-glycolylneuraminic acid; Neu5Gc) (55). As a result, human-specific differences evolved in the binding sites of human Siglecs, the family of sialic acid-binding proteins, for selective recognition of Neu5Ac over Neu5Gc (55). It is not known whether differences in the type of sialic acid contribute to the species barrier of prion transmission between animals and human. Nevertheless, it is tempting to speculate that upon cross-species transmission of prions to humans, enhanced sialylation of PrP^{Sc} "humanizes" prions of nonhuman origin, helping them to deceive the immune system.

Transmission of prions between species is more difficult than within the same species because of the species barrier. Remarkably, lymphoid tissues were found to be more susceptible to cross-species prion transmission than nerve tissues (15). Although the mechanisms behind high permissiveness of lymphoid tissues to prions are not known, prions acquired via cross-species transmission can persist stably and silently in SLOs for a long time in the absence of neuroinvasion (15, 56, 57). Aged animals that are known to be less susceptible to prion infection than young animals can also accumulate prions within their lymphoid tissues, despite lack of prions in their brains (58). Moreover, the lymphoid tissues display a higher capacity than nerve tissues to replicate prions after low-dose infection (59). The subclinical disease acquired via cross-species transmission or with low prion doses might never lead to neuroinvasion or clinical disease. Nevertheless, colonization of SLOs by prions poses a real risk due to the possibility of silent spread of infection through donation of blood or organs or infected surgical instruments (16, 56, 57, 60). The higher permissiveness of lymphoid tissues than the CNS is very surprising, considering that the expression level of PrP^{C} in lymphoid tissues is substantially lower than in brain (61–64) and that lymphoid cells are specialized in recognizing and degrading pathogens. Bearing in mind that sialylation status controls the lifetime of glycoclusters in blood circulation (65), our study suggests that enhanced sialylation of PrP^{Sc} in SLOs might contribute to the high permissiveness of lymphoid tissues to prions.

There are a number of mechanisms by which sialylation protects pathogens from the host (27). Among them is recruitment of factor H that dampens activation of alternative complement pathways by recognizing molecular patterns containing sialic acids on surfaces of host cells or pathogens (66, 67). Alternative mechanisms involve engaging inhibitory Siglecs (sialic acid recognizing Ig-like lectins) that likewise recognize sialic acid patterns and suppress innate immune cells (68, 69). In addition, sialylation can mask glycan ligands for Gal/GalNAc receptors or for galectins, a family of secreted proteins that recognize galactose and its derivatives (70). Finally, sialylation of glycans on the pathogen surface can inhibit production and/or binding of antibodies against asialoglycans (55). Of these four mechanisms, the first three could contribute to protection of prions due to enhanced PrP^{Sc} sialylation in SLOs.

Several types of cells—including macrophages, monocytes, B lymphocytes, and dendritic cells—capture prions at initial entry sites and transport them to SLOs (43, 71–73). In addition to trafficking of prions to SLOs, macrophages play a role in degrading prions (74–77). The present study suggests that, in addition to transporting and degrading prions, macrophages are also involved in sialylating PrP^{Sc}. Indeed, in vivo changes in sialylation patterns were observed in the peritoneal cavity, lymph nodes, and spleen—the sites with considerable populations of macrophages. Similar changes in PrP^{Sc} sialylation were also observed in vitro upon incubation of PrP^{Sc} with primary splenocytes or macrophage RAW cells. RAW cells showed significant ST activity on their surfaces. ST activity has also been found on the surface of dendritic cells and lymphocytes (48, 49). Considering that a number of cells of immune system—including B lymphocytes, monocytes, plasmacytoid dendritic cells, natural killer cells, and others—sequester and disseminate PrP^{Sc} (43, 72, 78), it is likely that sialylation of PrP^{Sc} is not limited to macrophages. Although degradation of PrP^{Sc} by macrophages has been well established, the present study suggests that macrophages might also play a protective role by enhancing sialylation of PrP^{Sc} in parallel to their role in degrading PrP^{Sc}. In a recent study, Siglec-1 (CD169) expressed on the surface of primary microphages was shown to be responsible for capturing sialylated viral pathogens and facilitating their intercellular transfer (79). It would be worth testing the possibility that enhanced sialylation of PrP^{Sc} in SLOs could also facilitate their intercellular transfer.

The present work suggests that enhanced sialylation of PrP^{Sc} occurs on the cell surface rather than intracellularly. Traditionally, STs were thought to localize exclusively within the intracellular secretory apparatus (50). A growing number of studies report ST activity in serum or on surfaces of the cells of immune system, including polymorphonuclear leukocyte, monocyte-derived dendritic cells, lymphocytes, and T cells (48, 49, 51–53, 80). Presence of ST on the cell surface or in serum allows rapid restoration or remodeling of the sialylation status of cells without de novo synthesis of cell surface glycoconjugates (48, 49, 81). ST expression and sialylation of cell surfaces are finely regulated during cell maturation, differentiation, and inflammation (48, 49, 81). Notably, systemic inflammatory response involves secretion of STs into serum, a process that modulates the inflammatory response (48, 81–83). It would be interesting to determine whether extracellular STs contribute to prion colonization of inflamed tissues via altering the sialylation status of PrP^{Sc}. Because the family of mammalian STs includes 20 enzymes that have redundant specificity (84), identifying those that are involved in enhancing sialylation of PrP^{Sc} would involve considerable effort.

If PrP^{Sc} is a subject of extracellular sialylation in SLOs, it is not clear why PrP^{C}, which is expressed on a cell surface, is not targeted by extracellular STs to the same extent as PrP^{Sc}. In mouse-derived primary splenocytes, the half-life of PrP^{C} was found to be only 1.5–2 h (85), which is much shorter than the half-life of PrP^{Sc}. In addition, the population of cells that express PrP^{C} could be different from the population of cells that express cell surface STs. In spleen and lymph nodes, PrP^{C} is primarily expressed by follicular dendritic cells (10), which are resident cells of germinal centers and different from dendritic cells of myeloid origin. It is not known whether follicular dendritic cells express cell surface STs.

Materials and Methods

Scrapie Materials. Weanling Golden Syrian hamsters or C57BL/6NHsd mice were inoculated intracranially or i.p. under 2% O_2/4 minimum alveolar concentration isoflurane anesthesia by using scrapie brain homogenates of hamster- or mouse-adapted strains, respectively. Animals were euthanized at the terminal stage of the disease, and organs were collected for 2D analysis. This study was carried out in strict accordance with the recommendations in the *Guide for the Care and Use of Laboratory Animals* of the National Institutes of Health (86). The animal protocol was approved by the Institutional Animal Care and Use Committee of the University of Maryland, Baltimore (Assurance no. A32000-01; Permit no.: 0215002).

Preparation of Brain and Spleen Materials for 2D. We prepared 10% (wt/vol) scrapie brain or spleen homogenates in PBS by using glass/Teflon homogenizers attached to a cordless 12-V compact drill (Ryobi) as described (87). For 2D electrophoresis of brain-derived material, an aliquot of 10% (wt/vol) homogenate was diluted with nine volumes of 1% (wt/vol) Triton X-100 in PBS, sonicated for 30 s inside Misonix S-4000 microplate horn (Qsonica), and treated with 20 μg/mL PK (New England BioLabs) for 30 min at 37 °C. For 2D electrophoresis of spleen-derived material, 250 μL of 10% (wt/vol) homogenate was diluted 1:1 with PBS, aliquotted into 0.2-mL thin-wall PCR tubes, sonicated for 30 s inside Misonix S-4000 microplate horn, and combined in one tube, which was subjected to a 30-min centrifugation at 16,000 × *g* at 4 °C. The pellet was resuspended in 25 μL of 1% (wt/vol) Triton in PBS and treated with 20 μg/mL PK for 30 min at 37 °C. Resulting brain or spleen samples were supplemented with 4× SDS loading buffer, heated for 10 min in a boiling water bath, and processed for 2D electrophoresis as described below.

Performance of 2D Electrophoresis. Samples of 25-μL volume prepared in loading buffer as described above were solubilized for 1 h at room temperature in 200 μL of solubilization buffer [8 M urea, 2% (wt/vol) CHAPS, 5 mM TBP, 20 mM Tris, pH 8.0), alkylated by adding 7 μL of 0.5 M iodoacetamide, and incubated for 1 h at room temperature. Then, 1,150 μL of ice-cold methanol was added, and samples were incubated for 2 h at −20 °C. After centrifugation at 16,000 × *g* at 4 °C, supernatant was discarded, and the pellet was resolubilized in 160 μL of rehydration buffer [7 M urea, 2 M thiourea, 1% (wt/vol) DTT, 1% (wt/vol) CHAPS, 1% (wt/vol) Triton X-100, 1% (vol/vol) ampholyte, and trace amount of Bromophenol Blue]. Fixed immobilized precast IPG (immobilized pH gradient) strips [catalog (cat.) no. ZM0018; Life Technologies] with a linear pH gradient 3–10 were rehydrated in 155 μL of resulting mixture overnight at room temperature inside IPG Runner cassettes (cat. no. ZM0008; Life Technologies). Isoelectrofocusing (first dimension separation) was performed at room temperature with rising voltage (175 V for 15 min, then 175–2,000-V linear gradient for 45 min, and then 2,000 V for 30 min) on Life Technologies Zoom Dual Power Supply using the XCell SureLock Mini-Cell Electrophoresis System (cat. no. EI0001; Life Technologies). The IPG strips were then equilibrated for 15 min consecutively in (*i*) 6 M urea, 20% (vol/vol) glycerol, 2% SDS, 375 mM Tris·HCl, pH 8.8, 130 mM DTT, and (*ii*) 6 M urea, 20% (vol/vol) glycerol, 2% SDS, 37 5mM Tris·HCl, pH 8.8, and 135 mM iodoacetamide, and loaded on 4–12% Bis-Tris ZOOM SDS/PAGE precast gels (cat. no. NP0330BOX; Life Technologies). For the second dimension, SDS/PAGE was performed for 1 h at 170 V. Immunoblotting was performed as described elsewhere; blots were stained by using 3F4 (cat. no. SIG-39600; Covance) antibody for hamster and ab3531 antibody (Abcam) for mouse tissues. To determine a specific 2D pattern and to check reproducibility of the procedure, at least two brains or spleens from for each animal group were analyzed.

Desialylation of PrP^{Sc} with Acetic Acid. PK-treated brain and spleen materials were prepared as for 2D electrophoresis. PK digestion was stopped by addition of 5 mM PMSF, then the samples were denatured by incubating for 10 min at 95 °C in the presence of 0.5% SDS and 40 mM DTT, followed by the addition of 1% (vol/vol) Nonidet P-40. Then the samples were supplemented with 1% (vol/vol) acetic acid and incubated at 100 °C for 1 h with 1,000 rpm shaking in Eppendorf thermomixer to achieve mild acid hydrolysis of sialic acids (80). Mock-treated samples were denatured by the same procedure, but not treated with acetic acid.

Desialylation of PrP^{Sc} with Sialidase. We diluted 10% (wt/vol) scrapie brain and spleen materials 10-fold in 1× PBS supplied with 1% (vol/vol) Triton X-100 and supplemented with 25 μg/mL PK. After 30 min at 37 °C, PK digestion was stopped by the addition of 5 mM PMSF. Then the samples were denatured by incubating for 10 min at 95 °C. The subsequent treatment with *Arthrobacter ureafaciens* sialidase (cat. no. P0722L; New England Biolabs) was as follows. After addition of 10% (vol/vol) sialidase buffer GlycoBuffer1 supplied by the enzyme manufacturer, 200 units/mL sialidase were added, followed by incubation on a shaker at 37 °C for 10–12 h. Mock-treated samples were processed by the same procedure, but not supplied with the sialidase.

Ion-Exchange Chromatography. We diluted 10% (wt/vol) 263K brain homogenates 10-fold in 25 mM Tris, pH 7.4, buffer supplied with 1% (wt/vol) Triton X-100 and sonicated for 30 s at 170 W energy output in the microplate horn (Misonix S-4000). The samples were then incubated with PK (10 μg/mL, 37 °C, 1 h) (cat. no. P8107S; New England Biolabs). The digestion was stopped by adding 2 mM PMSF. The samples were filtered through a 22-μm syringe filter (cat. no. SLGV033RB; Millipore). The cation or anion exchange mini columns (cat. no. 90008 and 90010, respectively; Thermo Scientific) were pre-equilibrated with Tris pH 7.4 and loaded with 400 μL of scrapie material prepared as described above, and centrifuged at 2,000 × *g* for 5 min. Then the columns were washed with 400 μL of Tris pH 7.4 buffer and centrifuged at 2,000 × *g* for 5 min. The columns were then washed consecutively with 400-μL volumes of the following concentrations of NaCl: 0.4, 0.8, 1.2, and 1.6 M prepared in Tris, pH 7.4. The material was collected by centrifugation, supplied with SDS sample buffer, heated for 10 min in a boiling water bath, and analyzed by SDS/PAGE or 2D electrophoresis.

Ultracentrifugation. We solubilized 10% (wt/vol) 263K brain homogenates by addition of 9 volumes of 10% (wt/vol) sarkosyl in PBS and sonication for 30 s inside a Misonix S-4000 microplate horn. The samples were precleared by 2 min centrifugation at 500 × *g* in a tabletop centrifuge, and then 100 μL of the supernatant were diluted with 900 μL PBS and centrifuged for 20 min at 20 °C at 32,400 rpm by using a TLA 100.3 rotor in an Optima TLX microultracentrifuge (Beckman). The supernatant containing solubilized PrP^{Sc} and the pellet containing insoluble PrP^{Sc} were collected. The pellet was resuspended in 200 μL of 1% (wt/vol) sarkosyl in PBS, treated with 20 μg/mL PK for 30 min at 37 °C, and supplemented with 4× SDS sample buffer. A total of 60 μL of the supernatant were treated with 20 μg/mL PK for 30 min at 37 °C, and concentrated by precipitation with 4 volumes of ice-cold acetone, incubated overnight at −20 °C and subsequently centrifuged for 30 min at 16,000 × *g*. The resulting pellet was resuspended in 1× SDS loading buffer.

Separation of PK-Sensitive and -Resistant PrP^{Sc}. We solubilized 10% (wt/vol) RML brain homogenates by addition of 9 volumes of 10% (wt/vol) sarkosyl in PBS and sonication for 30 s inside Misonix S-4000 microplate horn. The samples were precleared by 2 min centrifugation at 500 g in a tabletop centrifuge, and then 100 μL of the supernatant was diluted with 900 μL of PBS and centrifuged for 90 min at 16,000 × *g* at 4 °C. The supernatant containing solubilized PrP^{Sc} and the pellet containing insoluble PrP^{Sc} were collected. The pellet was resuspended in 50 μL of 1% (wt/vol) sarkosyl in PBS, treated with 20 μg/mL PK for 30 min at 37 °C, and supplemented with 4× SDS loading buffer. A total of 60 μL of the supernatant was treated with 2 or 20 μg/mL PK for 30 min at 37 °C, concentrated by precipitation with 4 volumes of ice-cold acetone, incubated overnight at −20 °C, and subsequently centrifuged for 30 min at 16,000 × *g*. The resulting pellet was resuspended in 1× SDS loading buffer.

IP Inoculation of Scrapie Material and Harvest of SLOs. We diluted 10% (wt/vol) 263K brain homogenate by using sterile PBS to a final concentration of 4% (wt/vol). A total of 500 μL per animal was injected i.p. into 4-wk-old C57BL/6NHsd mice by using 1-mL syringes with a 26-gauge needle (cat. no. 309625; BD Biosciences). After 6, 24, or 48 h after inoculations, spleens, mediastinal lymph nodes, and peritoneal cavity cells were collected. Spleens were homogenized to make 10% (wt/vol) tissue suspension in PBS with protease inhibitors (cOmplete, Mini, EDTA-free; cat. no. 04693159001; Roche) using glass/Teflon homogenizers. A total of 200 μL of 10% (wt/vol) spleen homogenate was diluted twice in PBS, sonicated for 30 s using Misonix S-4000 microplate horn sonicator and centrifuged at 16,000 × *g*, for 30 min at 4 °C. The pellet was collected and resuspended in 50 μL of PBS with 1% (wt/vol) Triton X-100 and 1 mM EDTA, then digested with PK (20 μg/mL, 37 °C, 30 min) and precipitated by acetone overnight as described above. The pellet was collected and dissolved in 30 μL of 1xSDS loading buffer, heated for 10 min in a boiling water bath and analyzed by 2D. Cells from the peritoneal cavity were collected and lysed as 1×10^6 cells per 200 μL of Mammalian Protein Extraction Reagent (M-PER) lysis buffer (cat. no. 78501; Thermo Scientific); the lysate was digested with PK (20 μg/mL, 37 °C, 30 min) and concentrated threefold by acetone precipitation. The pellet was dissolved in 1× SDS loading buffer, heated for 10 min in a boiling water bath, and analyzed by 2D. For mediastinal lymph nodes, the residual connective tissue was removed, and nodes were homogenized in PBS, 1% (wt/vol) Triton X-100, 1 mM EDTA with protease inhibitors using bead beater (Model 2412PS-12W-B30; Biospec Products) and 0.1-mm glass beads (cat. no. 11079101; Biospec Products). This suspension was centrifuged at 200 × *g* for 1 min to remove beads; supernatant was collected and digested with PK (20 μg/mL, 37 °C, 30 min). PrP^{Sc} in lymph node samples was enriched sixfold by acetone precipitation, and the enriched lysates were denatured in 1× SDS loading buffer, heated for 10 min in a boiling water bath, and analyzed by 2D. The experiment was repeated twice using two mice for each time point in each experiment.

Isolation of Mouse Primary Splenocytes. Healthy 5-wk-old female C57BL/6NHsd mice were euthanized with CO_2 inhalation. Dissected spleens were transferred to a 10-cm cell culture dish containing 10 mL of cold PBS with

2 mM EDTA and homogenized by using a plunger of a 5 mL syringe. Cell suspensions were collected in 15-mL tubes and centrifuged at 1,500 × *g* for 5 min. Red blood cells from the pellet were lysed by using RBC lysis buffer (cat. no. R7757; Sigma) as described by the manufacturer, then the cells were resuspended in cell culture medium DMEM (cat. no. 10-013-CV; Corning-Cellgro) supplemented with 10% (vol/vol) FBS (cat. no. 10082-147; Life Technologies), 1% (vol/vol) Glutamax (cat. no. 35050-061; Life Technologies), and 1% (wt/vol) antibiotics (cat. no. 15240-062; Life Technologies), and transferred to 25-cm^2 cell culture flasks (cat. no. SIAL0639; Sigma) for adherence. Nonadherent cells were removed; adherent cells were collected and checked for viability with trypan blue (cat. no. T8154; Sigma).

Culturing of RAW 264.7 Macrophages and Primary Splenocytes with PrP^{Sc}. RAW 264.7 cells or primary splenocytes were seeded in six-well plates (cat. no. 3506; Corning Costar) at densities of ∼1.5 × 10^5 or ∼0.8 × 10^6 cells per well, respectively, and cultured overnight in culture medium [DMEM, 10% (vol/vol) FBS, 1% (vol/vol) Glutamax, and 1% (wt/vol) antibiotics] at 37 °C and 5% CO_2 in humidified cell culture incubator. When RAW cells reached ∼50% confluence, the culture medium was changed to new medium containing 0.1% (wt/vol) 263K brain homogenate, cells were incubated for 2 h, then medium was removed, and cells were washed twice with prewarmed PBS to remove unbound PrP^{Sc} particles. Then, cells were cultured in culture medium [DMEM, 5% (vol/vol) FBS, 1% (vol/vol) Glutamax, and 1% (wt/vol) antibiotics] for 24 or 48 h. Cells were lysed in 200 μL of M-PER lysis buffer (cat. no. 78501; Thermo Scientific). A total of 90 μL of each lysate was treated with 20 μg/mL PK for 30 min at 37 °C under moderate shaking followed by precipitation overnight with acetone at −20 °C. Precipitated materials were centrifuged for 30 min at 16,000 × *g* at 4 °C. Pellets were air dried, dissolved in 30 μL of 1× SDS loading buffer, heated for 10 min in a boiling water bath, and analyzed by 2D.

In experiments with ST inhibitors, RAW 264.7 cells were incubated with 0.1% (wt/vol) 263K brain homogenate for 2 h and then washed as described above, and then CTP (cat. no. SIG-C1506; Sigma) or $3F_{ax}$-peracetyl Neu5Ac (cat. no. 566224; Millipore) was added to the medium to a final concentrations of 2 mM or 128 μM, respectively. Cells were cultured for 24 h in the presence of inhibitors and then harvested and analyzed as described above.

Flow Cytometry Analysis of ST Activity on RAW Cells. A fluorescent precursor CMP-5-FITC-NEU was prepared and used as described with minor modifications (48, 49, 88). RAW cells were suspended at 5 × 10^5 cells per 100 μL of serum-free medium. For neuraminidase treatment, cells were suspended at 5 × 10^6 per mL into 300 μL of serum free medium and treated with 200 unit/mL *Clostridium perfringens* neuraminidase (α2–3,6,8 neuraminidase, cat. no. P0720L; New England Biolabs) for 90 min at 37 °C in CO_2 incubator. After treatment, cells were washed with serum-free medium and divided into tubes containing 100 μL of serum-free medium at a density of 5 × 10^5 cells per tube. CMP-5-FITC-NEU was added to neuraminidase-treated or untreated cells to a final concentration of 10 μM, and cells were incubated for 2 h at 37 °C in a CO_2 incubator with gentle intermittent shaking. In experiments with ST inhibitor, neuraminidase-treated or nontreated RAW cells were incubated with 5 mM CTP for 30 min before addition of CMP-5-FITC-NEU, and 5 mM CTP was maintained in culture medium during 2-h incubations with CMP-5-FITC-NEU. After incubation with CMP-5-FITC-NEU, 1 mL of cold serum-free medium was added to cells, and the cells were washed with serum-free medium to remove unbound fluorescent precursor. Cells were centrifuged at 1,000 × *g* for 3 min, and then the pellet was collected and suspended in 400 μL of PBS with 1% (wt/vol) BSA and 2 mM EDTA for FACS analysis. Cells, untreated with neither neuraminidase nor CMP-5-FITC-NEU, served as an autofluorescence control. The data were collected on FITC channel by using a BD FACS CANTO II instrument and analyzed by using Flow Jo software (Version 8.8.7).

Statistical Analysis of Sialylation on 2D. The 2D Western blot signal intensity was digitized for densitometry analysis by using AlphaView software (ProteinSimple). The 2D blots were aligned horizontally, and a line drawn at pI 7.5 was used to arbitrarily separate diglycosylated charge isoforms into hypersialylated and hyposialylated (Fig. S1). In the software window, a rectangle was drawn to confine the spots of interest, and the densities were measured. The intensity of an equal background area from the same blot was subtracted before calculations were performed. The acquired spot ensemble intensities were used to calculate percentage of "hypersialylated" isoforms. Hypersialylated isoforms were defined operationally as all isoforms located to the left of the pI-7.5 line; the percentage of hypersialylated isoforms was calculated assuming the total intensity of all isoforms as 100%. Results are presented as the mean ± SD. Statistical significance (*P*) between groups were calculated by Student's *t* test and is indicated in figures as * for significant ($P < 0.05$) and # for insignificant ($P > 0.05$) statistics.

ACKNOWLEDGMENTS. We thank Pamela Wright for editing the manuscript. Flow-cytometry analyses were performed at the University of Maryland Marlene and Stewart Greenebaum Cancer Center Flow Cytometry Shared Service. This work was supported by National Institutes of Health Grants R01 NS045585 and R01 NS074998.

1. Prusiner SB (1982) Novel proteinaceous infectious particles cause scrapie. *Science* 216(4542):136–144.
2. Legname G, et al. (2004) Synthetic mammalian prions. *Science* 305(5684):673–676.
3. Cohen FE, Prusiner SB (1998) Pathologic conformations of prion proteins. *Annu Rev Biochem* 67:793–819.
4. Aguzzi A, Nuvolone M, Zhu C (2013) The immunobiology of prion diseases. *Nat Rev Immunol* 13(12):888–902.
5. Sigurdson CJ, et al. (1999) Oral transmission and early lymphoid tropism of chronic wasting disease PrPres in mule deer fawns (Odocoileus hemionus). *J Gen Virol* 80(Pt 10):2757–2764.
6. Hilton DA, Fathers E, Edwards P, Ironside JW, Zajicek J (1998) Prion immunoreactivity in appendix before clinical onset of variant Creutzfeldt-Jakob disease. *Lancet* 352(9129): 703–704.
7. Andréoletti O, et al. (2000) Early accumulation of PrP(Sc) in gut-associated lymphoid and nervous tissues of susceptible sheep from a Romanov flock with natural scrapie. *J Gen Virol* 81(Pt 12):3115–3126.
8. McCulloch L, et al. (2011) Follicular dendritic cell-specific prion protein (PrP) expression alone is sufficient to sustain prion infection in the spleen. *PLoS Pathog* 7(12): e1002402.
9. Kujala P, et al. (2011) Prion uptake in the gut: Identification of the first uptake and replication sites. *PLoS Pathog* 7(12):e1002449.
10. Brown KL, et al. (1999) Scrapie replication in lymphoid tissues depends on prion protein-expressing follicular dendritic cells. *Nat Med* 5(11):1308–1312.
11. Montrasio F, et al. (2000) Impaired prion replication in spleens of mice lacking functional follicular dendritic cells. *Science* 288(5469):1257–1259.
12. Glatzel M, Heppner FL, Albers KM, Aguzzi A (2001) Sympathetic innervation of lymphoreticular organs is rate limiting for prion neuroinvasion. *Neuron* 31(1): 25–34.
13. Mabbott NA, Mackay F, Minns F, Bruce ME (2000) Temporary inactivation of follicular dendritic cells delays neuroinvasion of scrapie. *Nat Med* 6(7):719–720.
14. Prinz M, et al. (2003) Positioning of follicular dendritic cells within the spleen controls prion neuroinvasion. *Nature* 425(6961):957–962.
15. Béringue V, et al. (2012) Facilitated cross-species transmission of prions in extraneural tissue. *Science* 335(6067):472–475.
16. Peden AH, Head MW, Ritchie DL, Bell JE, Ironside JW (2004) Preclinical vCJD after blood transfusion in a PRNP codon 129 heterozygous patient. *Lancet* 364(9433): 527–529.
17. Hilton DA, et al. (2004) Prevalence of lymphoreticular prion protein accumulation in UK tissue samples. *J Pathol* 203(3):733–739.
18. Heikenwalder M, et al. (2005) Chronic lymphocytic inflammation specifies the organ tropism of prions. *Science* 307(5712):1107–1110.
19. Seeger H, et al. (2005) Coincident scrapie infection and nephritis lead to urinary prion excretion. *Science* 310(5746):324–326.
20. Turk E, Teplow DB, Hood LE, Prusiner SB (1988) Purification and properties of the cellular and scrapie hamster prion proteins. *Eur J Biochem* 176(1):21–30.
21. Endo T, Groth D, Prusiner SB, Kobata A (1989) Diversity of oligosaccharide structures linked to asparagines of the scrapie prion protein. *Biochemistry* 28(21): 8380–8388.
22. Stimson E, Hope J, Chong A, Burlingame AL (1999) Site-specific characterization of the N-linked glycans of murine prion protein by high-performance liquid chromatography/electrospray mass spectrometry and exoglycosidase digestions. *Biochemistry* 38(15):4885–4895.
23. Novitskaya V, Makarava N, Sylvester I, Bronstein IB, Baskakov IV (2007) Amyloid fibrils of mammalian prion protein induce axonal degeneration in NTERA2-derived terminally differentiated neurons. *J Neurochem* 102(2):398–407.
24. Stahl N, et al. (1993) Structural studies of the scrapie prion protein using mass spectrometry and amino acid sequencing. *Biochemistry* 32(8):1991–2002.
25. Rudd PM, et al. (1999) Glycosylation differences between the normal and pathogenic prion protein isoforms. *Proc Natl Acad Sci USA* 96(23):13044–13049.
26. Varki A, Gagneux P (2012) Multifarious roles of sialic acids in immunity. *Ann N Y Acad Sci* 1253:16–36.
27. Varki A (2011) Since there are PAMPs and DAMPs, there must be SAMPs? Glycan "self-associated molecular patterns" dampen innate immunity, but pathogens can mimic them. *Glycobiology* 21(9):1121–1124.
28. Brown GC, Neher JJ (2014) Microglial phagocytosis of live neurons. *Nat Rev Neurosci* 15(4):209–216.
29. Savill J, Dransfield I, Gregory C, Haslett C (2002) A blast from the past: Clearance of apoptotic cells regulates immune responses. *Nat Rev Immunol* 2(12):965–975.

30. Aminoff D, Bruegge WF, Bell WC, Sarpolis K, Williams R (1977) Role of sialic acid in survival of erythrocytes in the circulation: Interaction of neuraminidase-treated and untreated erythrocytes with spleen and liver at the cellular level. *Proc Natl Acad Sci USA* 74(4):1521–1524.
31. Jansen AJG, et al. (2012) Desialylation accelerates platelet clearance after refrigeration and initiates GPIbα metalloproteinase-mediated cleavage in mice. *Blood* 119(5):1263–1273.
32. Linnartz B, Kopatz J, Tenner AJ, Neumann H (2012) Sialic acid on the neuronal glycocalyx prevents complement C1 binding and complement receptor-3-mediated removal by microglia. *J Neurosci* 32(3):946–952.
33. Witting A, Müller P, Herrmann A, Kettenmann H, Nolte C (2000) Phagocytic clearance of apoptotic neurons by microglia/brain macrophages in vitro: Involvement of lectin-, integrin-, and phosphatidylserine-mediated recognition. *J Neurochem* 75(3):1060–1070.
34. Varki A (2008) Sialic acids in human health and disease. *Trends Mol Med* 14(8): 351–360.
35. Lewis AL, et al. (2009) Innovations in host and microbial sialic acid biosynthesis revealed by phylogenomic prediction of nonulosonic acid structure. *Proc Natl Acad Sci USA* 106(32):13552–13557.
36. Silveira JR, et al. (2005) The most infectious prion protein particles. *Nature* 437(7056): 257–261.
37. Stahl N, et al. (1992) Glycosylinositol phospholipid anchors of the scrapie and cellular prion proteins contain sialic acid. *Biochemistry* 31(21):5043–5053.
38. Katorcha E, Makarava N, Savtchenko R, D'Azzo A, Baskakov IV (2014) Sialylation of prion protein controls the rate of prion amplification, the cross-species barrier, the ratio of PrPSc glycoform and prion infectivity. *PLoS Pathog* 10(9):e1004366.
39. Makarava N, et al. (2012) A new mechanism for transmissible prion diseases. *J Neurosci* 32(21):7345–7355.
40. Parchi P, et al. (2000) Genetic influence on the structural variations of the abnormal prion protein. *Proc Natl Acad Sci USA* 97(18):10168–10172.
41. Sajnani G, Pastrana MA, Dynin I, Onisko B, Requena JR (2008) Scrapie prion protein structural constraints obtained by limited proteolysis and mass spectrometry. *J Mol Biol* 382(1):88–98.
42. Notari S, et al. (2004) Effects of different experimental conditions on the PrPSc core generated by protease digestion: Implications for strain typing and molecular classification of CJD. *J Biol Chem* 279(16):16797–16804.
43. Castro-Seoane R, et al. (2012) Plasmacytoid dendritic cells sequester high prion titres at early stages of prion infection. *PLoS Pathog* 8(2):e1002538.
44. Klohs WD, Bernacki RJ, Korytnyk W (1979) Effects of nucleotides and nucleotide: Analogs on human serum sialyltransferase. *Cancer Res* 39(4):1231–1238.
45. Ortiz AI, Reglero A, Rodríguez-Aparicio LB, Luengo JM (1989) In vitro synthesis of colominic acid by membrane-bound sialyltransferase of *Escherichia coli* K-235. Kinetic properties of this enzyme and inhibition by CMP and other cytidine nucleotides. *Eur J Biochem* 178(3):741–749.
46. Burkart MD, et al. (2000) Chemo-enzymatic synthesis of fluorinated sugar nucleotide: Useful mechanistic probes for glycosyltransferases. *Bioorg Med Chem* 8(8):1937–1946.
47. Rillahan CD, et al. (2012) Global metabolic inhibitors of sialyl- and fucosyltransferases remodel the glycome. *Nat Chem Biol* 8(7):661–668.
48. Rifat S, et al. (2008) Expression of sialyltransferase activity on intact human neutrophils. *J Leukoc Biol* 84(4):1075–1081.
49. Cabral MG, et al. (2010) Human dendritic cells contain cell surface sialyltransferase activity. *Immunol Lett* 131(1):89–96.
50. Harduin-Lepers A, et al. (2001) The human sialyltransferase family. *Biochimie* 83(8): 727–737.
51. Gross HJ, Merling A, Moldenhauer G, Schwartz-Albiez R (1996) Ecto-sialyltransferase of human B lymphocytes reconstitutes differentiation markers in the presence of exogenous CMP-N-acetyl neuraminic acid. *Blood* 87(12):5113–5126.
52. Kaufmann M, et al. (1999) Identification of an alpha2,6-sialyltransferase induced early after lymphocyte activation. *Int Immunol* 11(5):731–738.
53. Schwartz-Albiez R, Merling A, Martin S, Haas R, Gross HJ (2004) Cell surface sialylation and ecto-sialyltransferase activity of human CD34 progenitors from peripheral blood and bone marrow. *Glycoconj J* 21(8-9):451–459.
54. Gross HJ (1992) Fluorescent CMP-sialic acids as a tool to study the specificity of the CMP-sialic acid carrier and the glycoconjugate sialylation in permeabilized cells. *Eur J Biochem* 203(1-2):269–275.
55. Varki A (2010) Colloquium paper: Uniquely human evolution of sialic acid genetics and biology. *Proc Natl Acad Sci USA* 107(Suppl 2):8939–8946.
56. Bishop MT, et al. (2013) Prion infectivity in the spleen of a PRNP heterozygous individual with subclinical variant Creutzfeldt-Jakob disease. *Brain* 136(Pt 4):1139–1145.
57. Peden A, et al. (2010) Variant CJD infection in the spleen of a neurologically asymptomatic UK adult patient with haemophilia. *Haemophilia* 16(2):296–304.
58. Brown KL, Mabbott NA (2014) Evidence of subclinical prion disease in aged mice following exposure to bovine spongiform encephalopathy. *J Gen Virol* 95(Pt 1): 231–243.
59. Halliez S, et al. (2014) Accelerated, spleen-based titration of variant Creutzfeldt-Jakob disease infectivity in transgenic mice expressing human prion protein with sensitivity comparable to that of survival time bioassay. *J Virol* 88(15):8678–8686.
60. Wroe SJ, et al. (2006) Clinical presentation and pre-mortem diagnosis of variant Creutzfeldt-Jakob disease associated with blood transfusion: A case report. *Lancet* 368(9552):2061–2067.
61. Peralta OA, Eyestone WH (2009) Quantitative and qualitative analysis of cellular prion protein (PrP(C)) expression in bovine somatic tissues. *Prion* 3(3):161–170.
62. Ford MJ, Burton LJ, Morris RJ, Hall SM (2002) Selective expression of prion protein in peripheral tissues of the adult mouse. *Neuroscience* 113(1):177–192.
63. Horiuchi M, Yamazaki N, Ikeda T, Ishiguro N, Shinagawa M (1995) A cellular form of prion protein (PrPC) exists in many non-neuronal tissues of sheep. *J Gen Virol* 76(Pt 10):2583–2587.
64. Clouse MD, Shikiya RA, Bartz JC, Kincaid AE (2015) Nasal associated lymphoid tissue of the Syrian golden hamster expresses high levels of PrPC. *PLoS One* 10(2):e0117935.
65. Tanaka K, et al. (2010) Noninvasive imaging of dendrimer-type N-glycan clusters: in vivo dynamics dependence on oligosaccharide structure. *Angew Chem Int Ed Engl* 49(44):8195–8200.
66. Pangburn MK, Pangburn KL, Koistinen V, Meri S, Sharma AK (2000) Molecular mechanisms of target recognition in an innate immune system: Interactions among factor H, C3b, and target in the alternative pathway of human complement. *J Immunol* 164(9): 4742–4751.
67. Kajander T, et al. (2011) Dual interaction of factor H with C3d and glycosaminoglycans in host-nonhost discrimination by complement. *Proc Natl Acad Sci USA* 108(7): 2897–2902.
68. Carlin AF, et al. (2009) Molecular mimicry of host sialylated glycans allows a bacterial pathogen to engage neutrophil Siglec-9 and dampen the innate immune response. *Blood* 113(14):3333–3336.
69. Cao H, Crocker PR (2011) Evolution of CD33-related siglecs: Regulating host immune functions and escaping pathogen exploitation? *Immunology* 132(1):18–26.
70. Vasta GR (2009) Roles of galectins in infection. *Nat Rev Microbiol* 7(6):424–438.
71. Huang FP, Farquhar CF, Mabbott NA, Bruce ME, MacPherson GG (2002) Migrating intestinal dendritic cells transport PrP(Sc) from the gut. *J Gen Virol* 83(Pt 1):267–271.
72. Michel B, et al. (2012) Incunabular immunological events in prion trafficking. *Sci Rep* 2:440.
73. Takakura I, et al. (2011) Orally administered prion protein is incorporated by m cells and spreads into lymphoid tissues with macrophages in prion protein knockout mice. *Am J Pathol* 179(3):1301–1309.
74. Beringue V, et al. (2000) Role of spleen macrophages in the clearance of scrapie agent early in pathogenesis. *J Pathol* 190(4):495–502.
75. Carp RI, Callahan SM (1981) In vitro interaction of scrapie agent and mouse peritoneal macrophages. *Intervirology* 16(1):8–13.
76. Sassa Y, Inoshima Y, Ishiguro N (2010) Bovine macrophage degradation of scrapie and BSE PrPSc. *Vet Immunol Immunopathol* 133(1):33–39.
77. Sassa Y, Yamasaki T, Horiuchi M, Inoshima Y, Ishiguro N (2010) The effects of lysosomal and proteasomal inhibitors on abnormal forms of prion protein degradation in murine macrophages. *Microbiol Immunol* 54(12):763–768.
78. Klein MA, et al. (1997) A crucial role for B cells in neuroinvasive scrapie. *Nature* 390(6661):687–690.
79. Erikson E, et al. (2015) Mouse Siglec-1 mediates trans-infection of surface-bound murine leukemia virus in a sialic acid N-acyl side chain-dependent manner. *J Biol Chem*, jbc.M115.681338, in press.
80. Nasirikenari M, Veillon L, Collins CC, Azadi P, Lau JT (2014) Remodeling of marrow hematopoietic stem and progenitor cells by non-self ST6Gal-1 sialyltransferase. *J Biol Chem* 289(10):7178–7189.
81. Crespo HJ, Lau JTY, Videira PA (2013) Dendritic cells: A spot on sialic acid. *Front Immunol* 4:491.
82. Kaplan HA, Woloski BM, Hellman M, Jamieson JC (1983) Studies on the effect of inflammation on rat liver and serum sialyltransferase. Evidence that inflammation causes release of Gal beta 1 leads to 4GlcNAc alpha 2 leads to 6 sialyltransferase from liver. *J Biol Chem* 258(19):11505–11509.
83. Jamieson JC, McCaffrey G, Harder PG (1993) Sialyltransferase: A novel acute-phase reactant. *Comp Biochem Physiol B* 105(1):29–33.
84. Takashima S (2008) Characterization of mouse sialyltransferase genes: Their evolution and diversity. *Biosci Biotechnol Biochem* 72(5):1155–1167.
85. Parizek P, et al. (2001) Similar turnover and shedding of the cellular prion protein in primary lymphoid and neuronal cells. *J Biol Chem* 276(48):44627–44632.
86. Committee on Care and Use of Laboratory Animals (1996) *Guide for the Care and Use of Laboratory Animals* (Natl Inst Health, Bethesda), DHHS Publ No (NIH) 85-23.
87. Makarava N, et al. (2012) Stabilization of a prion strain of synthetic origin requires multiple serial passages. *J Biol Chem* 287(36):30205–30214.
88. Brossmer R, Gross HJ (1994) Fluorescent and photoactivatable sialic acids. *Methods Enzymol* 247:177–193.